# Understanding Hydrogen Sorption in a Metal–Organic Framework with Open-Metal Sites and Amide Functional Groups

**ARTICLE** *in* THE JOURNAL OF PHYSICAL CHEMISTRY C · APRIL 2013

Impact Factor: 4.77 · DOI: 10.1021/jp402304a



**8 AUTHORS**, INCLUDING:

Tony Pham
University of South Florida
**36** PUBLICATIONS **702** CITATIONS
SEE PROFILE

Youssef Belmabkhout
King Abdullah University of Science and Techn…
**58** PUBLICATIONS **2,454** CITATIONS
SEE PROFILE

Brian Space
University of South Florida
**91** PUBLICATIONS **1,947** CITATIONS
SEE PROFILE

THE JOURNAL OF PHYSICAL CHEMISTRY C

Article

pubs.acs.org/JPCC

# Understanding Hydrogen Sorption in a Metal–Organic Framework with Open-Metal Sites and Amide Functional Groups

Tony Pham,[†,‡] Katherine A. Forrest,[†,‡] Patrick Nugent,[†] Youssef Belmabkhout,[§] Ryan Luebke,[§] Mohamed Eddaoudi,[†,§] Michael J. Zaworotko,[†] and Brian Space*[,†]

[†]Department of Chemistry, University of South Florida, 4202 East Fowler Avenue, CHE205, Tampa, Florida 33620-5250, United States

[§]Advanced Membranes and Porous Materials Center, Division of Physical Sciences and Engineering 4700, King Abdullah University of Science and Technology (KAUST), Thuwal 23955-6900, Kingdom of Saudi Arabia

Supporting Information

**ABSTRACT:** Grand canonical Monte Carlo (GCMC) studies of the mechanism of hydrogen sorption in an *rht*-MOF known as Cu-TPBTM are presented. The MOF is a decorated/substituted isostructural analogue to the unembellished *rht*-MOF, PCN-61, that was studied previously [Forrest, K. A. et al. *J. Phys. Chem. C* **2012**, *116*, 15538−15549.]. The simulations were performed using three different hydrogen potentials of increasing complexity. Simulated hydrogen sorption isotherms and calculated isosteric heat of adsorption, $Q_{st}$, values were in excellent agreement with the reported experimental data for only a polarizable model in one of four experimentally observed crystal structure configurations. The study demonstrates the ability of modeling to distinguish the differential sorption of distinct strucures; one configuration is found to be dominant due to favorable interactions with substrates. In addition, it was discovered that the presence of polar amide groups had a significant effect on the electrostatics of the $Cu^{2+}$ ions and directs the low-pressure physisorption of hydrogen in the MOF. This is in contrast to what was observed in PCN-61, where an exterior copper ion had a higher relative charge and was the favored loading site. This tunability of the electrostatics of the copper ions via chemical substitution on the MOF framework can be explained by the presence of the negatively charged oxygen atom of the amide group that causes the interior $Cu^{2+}$ ion to exhibit a higher positive charge through an inductive effect. Further, control simulations, taking advantage of the flexibility afforded by theoretical modeling, include artificially modified charges for both $Cu^{2+}$ ions chosen equal to or with a higher charge on the exterior $Cu^{2+}$ ion. This choice resulted in distinctly different hydrogen sorption characteristics in Cu-TPBTM with no direct sorption on the open-metal sites. Thus, this study demonstrates both the tunable nature of MOF platforms and the possibility for rational design of sorption/catalytic sites and characteristics through the active interplay of theory and experiment. The ability of accurate, carefully parametrized and transferable force fields to model and predict small molecule sorption in MOFs, even including open-metal sites, is demonstrated.

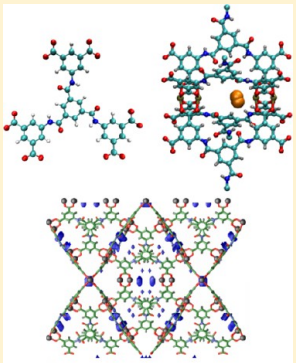

## I. INTRODUCTION

Molecular hydrogen, $H_2$, is greatly recognized as a clean alternative fuel; it has a relatively high energy capacity and the combustion of hydrogen in an engine or fuel cell releases only water as a byproduct.[1] The ultimate U.S. Department of Energy (DOE) target for a potential on-board hydrogen storage system at near-ambient temperatures and pressures (e.g., 298 K and 100 atm) is 7.5 wt % (0.075 kg/kg) or 0.070 kg/L.[2] In addition to raw uptake capacity, the storage system and fueling cost must be low, and the hydrogen uptake process must be totally reversible with the recharging of hydrogen being completed within a few minutes, comparable to the use of liquid fuels such as diesel or gasoline. Porous materials that physisorb hydrogen seems to offer the greatest advantage as a hydrogen storage system since they can sorb a considerable amount of hydrogen in the pores as well as having a fast charge−recharge process.

Metal−organic frameworks (MOFs) are crystalline compounds that have been shown to be promising for applications in hydrogen storage.[1,3,4] MOFs represent a group of periodic structures that are composed of organic linkers coordinated to metal ions.[5] They can be synthesized to have large surface areas and can be assembled from molecular building blocks (MBB) with desired/tunable chemical functionality.[6] This building block approach[7,8] has led to the design and synthesis of a highly successful platform of MOFs, known as *rht*-MOFs.[8−19] These MOFs have an *rht* topology (*rht* stands for "rhombicuboctahedron"), which is characterized by having 24 edges of a cuboctahedron connecting with a linker having $C_3$ symmetry.[10] Such linkers are hexatopic and consist of three coplanar isophthalate-based moieties.[10,11] When these *rht*-MOFs are synthesized, the resulting framework consists of three distinct cages (cuboctahedron, truncated tetrahedron, and truncated octahedron), a feature that makes them different from other MOF platforms. *rht*-MOFs are promising because they have

**Received:** March 6, 2013
**Revised:** April 12, 2013
**Published:** April 12, 2013

high surface areas and contains open-metal sites and tunable pores (size and functionality).

Computational studies involving both electronic structure methods and molecular mechanics, in addition to inelastic neutron scattering and X-ray diffraction studies have added insights to MOFs and the mechanism of hydrogen sorption.[1,3] Recently, computational studies involving Grand canonical Monte Carlo (GCMC) methods were performed to investigate hydrogen sorption in an *rht*-MOF known as PCN-61.[20] PCN-61 (PCN stands for porous coordination network) is a *rht*-MOF composed of 5,5′,5″-benzene-1,3,5-triyltris(1-ethynl-2-isophthalate) (btei) linkers coordinated to $Cu^{2+}$ ions.[10,11] The MOF has an estimated BET surface area of 3000 $m^2\,g^{-1}$ (Langmuir surface area = 3500 $m^2\,g^{-1}$) and a pore volume of 1.36 $cm^3\,g^{-1}$. Experimental studies have shown that PCN-61 has a hydrogen uptake of 2.25 wt % at 77 K and 1.0 atm. Note, although the DOE targets for hydrogen storage are for systems operating at near-ambient temperatures and pressures, the hydrogen uptake values at 77 K and 1.0 atm have been widely investigated and commonly used as benchmarks to compare the hydrogen uptake capacities of different MOFs.[1,4]

In the computational studies,[20] hydrogen sorption in PCN-61 was simulated using three different hydrogen potentials of increasing anisotropy to investigate the effects that van der Waals repulsion/dispersion interactions, charge-quadrupole interactions, and many-body polarization effects have on the physisorption of hydrogen in this MOF. The three hydrogen potentials are known as Buch,[21] BSS,[22] and BSSP,[22] respectively. It was shown that the simulated hydrogen sorption isotherms and associated isosteric heats of adsorption, $Q_{st}$, were in quantitative agreement with experiment only for the model with explicit polarization.[20] Furthermore, the inclusion of many-body polarization affected the $H_2$ molecule orientation and distance about the open-metal sites and enhanced charge-quadrupole interactions. Analysis of the 3-D histrograms inside PCN-61 revealed three distinct dipolar hydrogen populations for the polarizable model: the open metal site located in the cuboctahedron, the corner of the truncated tetrahedron, and the corner of the truncated octahedron. A key result from the study showed that many-body polarization cannot be neglected when considering high-density hydrogen interacting with highly polar MOFs. Moreover, it was demonstrated that many-body polarization had a major effect on the sorption of hydrogen in PCN-61 and correctly describes the interactions between the hydrogen molecules and the open-metal sites.[20,23,24]

In this study, we use similar GCMC methods to investigate hydrogen sorption in a decorated isostructural analogue of PCN-61, known as Cu-TPBTM (Figure 1).[12] This *rht*-MOF was constructed with *N*,*N*′*N*″-tris(isophthalyl)-1,3,5-benzene-tricarboxamide (TPBTM) as the organic linker. The linker in Cu-TPBTM contains amide functional groups in place of alkyne groups that were seen in PCN-61. Cu-TPBTM has an estimated BET surface area of 3160 $m^2\,g^{-1}$ (Langmuir surface area = 3570 $m^2\,g^{-1}$) and a pore volume of 1.27 $cm^3\,g^{-1}$. This MOF was shown to have one of the highest uptakes for $CO_2$ sorption. Recently, we chose PCN-61 for the computational studies due to the potential utility of *rht*-MOFs and as the use of a prototype structure for baseline computational studies.[20] In this study, Cu-TPBTM was chosen to investigate the effects that a polar functional group on the organic linker has on the physisorption of hydrogen in *rht*-MOFs. Specifically, the effect of substituting a nonpolar functional group with a polar functional group on hydrogen sorption in a *rht*-MOF (from alkyne in PCN-61 to amide in Cu-TPBTM) will be addressed. Further, these studies represent a systematic approach to understanding small molecule sorption in chemically tunable MOFs that promote strong intermolecular interactions (with open-metal sites and polar frameworks). Thus, such MOFs offer a challenge for theoretical-experimental cooperation in design, evaluation and modification of candidate MOF platforms. Evaluating Cu-TPBTM thus serves the dual purpose of investigating $H_2$ storage mechanisms in a MOF sorption

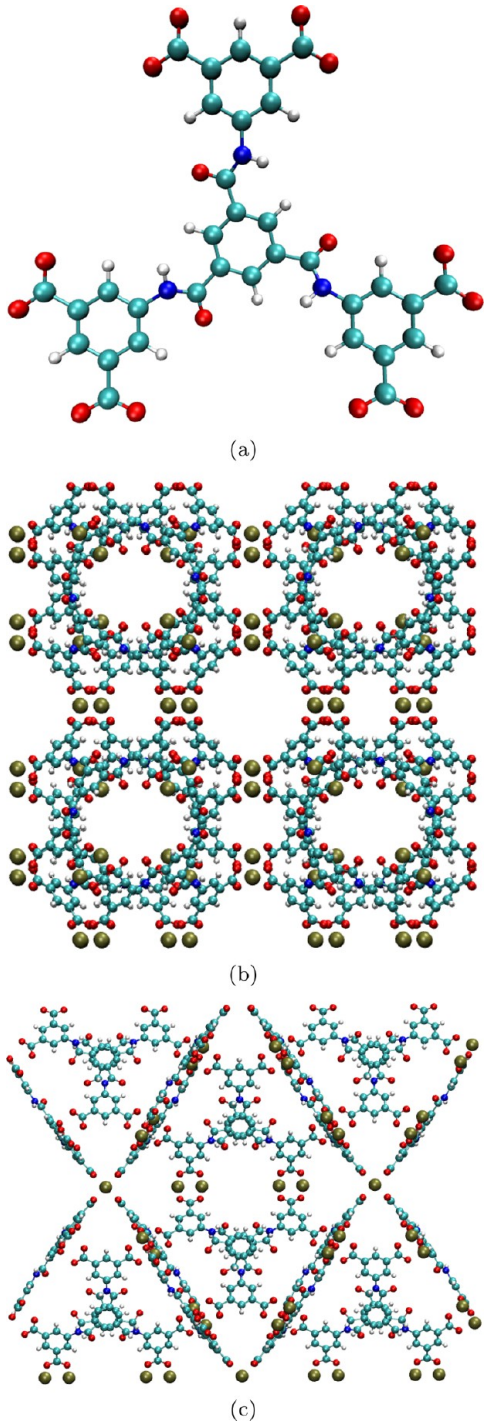


**Figure 1.** Molecular view of Cu-TPBTM. (a) TPBTM linker. (b) Side view of unit cell. (c) Corner view of unit cell. Atom colors: C = cyan, H = white, N = blue, O = red, Cu = tan.


dx.doi.org/10.1021/jp402304a | *J. Phys. Chem. C* 2013, 117, 9340−9354

system that is well characterized and amenable to careful modeling.

Herein, we report results of experimental hydrogen sorption studies in Cu-TPBTM that includes low-pressure absolute sorption isotherms and $Q_{st}$ values. The experimental low-pressure hydrogen sorption isotherm of Cu-TPBTM shows that the MOF is capable of sorbing 2.61 wt % at 77 K and 1.0 atm. It is not surprising that Cu-TPBTM sorbs more $H_2$ than PCN-61 at low-pressures because the presence of the polar amide groups in the MOF enhances $H_2$ binding affinity. In addition, Cu-TPBTM exhibits a smaller unit cell length than PCN-61 (42.153 vs 42.796 Å), which leads to narrower pore sizes. Smaller pore sizes would allow the molecules to interact with more atoms of the framework simultaneously.[11,20,25] Like PCN-61, it is shown herein that many-body polarization has a major effect on hydrogen sorption in Cu-TPBTM. However, the results obtained for Cu-TPBTM extend beyond the necessity to include polarization for modeling hydrogen sorption in highly charged/polar MOFs. A total of four different configurations were observed in the crystal structure of Cu-TPBTM that alter only in the orientation of the central aromatic ring and the amide group of the linker. This study demonstrates that one of the configurations is much more favorable toward hydrogen sorption than the others due to both steric and electrostatic effects. Further, empirical measurements were quantitatively reproduced in only one of the experimentally observed configurations. This strongly suggests that hydrogen sorption induces the crystal to dynamically adopt the configuration favorable to sorption.

Further, it was observed that the presence of the amide groups in Cu-TPBTM changes the electrostatic nature of the $Cu^{2+}$ ions of the Cu paddlewheels relative to PCN-61. In PCN-61, it was shown that the exterior $Cu^{2+}$ ion (the ion furthest from the center of the linker) had the higher charge of the two $Cu^{2+}$ ions.[20] In contrast, the presence of the electronegative oxygen atom of the amide group on the linker in Cu-TPBTM causes the interior $Cu^{2+}$ ion (the ion closest to the center of the linker) to exhibit the higher positive charge, and also causes the charge of the exterior $Cu^{2+}$ ion to decrease. As a result, the mechanism of hydrogen sorption in the MOF changes and a different initial sorption site was observed. It was demonstrated in our studies on PCN-61 and Cu-TPBTM that substituting one moiety in the organic linker of an *rht*-MOF changes the initial binding site for hydrogen sorption. This leads to the potential for rational design in synthesis where one can control which site the sorbate binds to upon initial loading by making a simple chemical modification.

Furthermore, control simulations were performed to assess the importance of having a highly accurate and transferable force field for the MOF and sorbates to describe the correct sorption behavior upon simulation with many-body polarization effects. Although the interior $Cu^{2+}$ ion was calculated to have the higher charge of the two $Cu^{2+}$ ions from quantum-mechanical calculations, the simulations were also performed in situations where the $Cu^{2+}$ ions were the same charge and where the exterior $Cu^{2+}$ ion had the higher charge. It was shown that the simulations involving these test cases did not capture the sorption of hydrogen onto the open-metal site in Cu-TPBTM.

## II. COMPUTATIONAL METHODS

**A. Molecular Simulation Parameters.** Analysis of the crystallographic structure of Cu-TPBTM at room temperature revealed two distinct configurations of the framework: A and B (Figure 2).[12] These two configurations differ in the position of the atoms in the amide group and the central aromatic ring of the TPBTM linker and corresponding collective puckering of the rings shown in Figure 2. The parametrizations and simulations were performed on both of these configurations of the framework and the corresponding results are shown herein. It will be demonstrated that simulating configuration A alone reproduces the observed $H_2$ sorption in Cu-TPBTM. Note, in configuration A, the amide oxygen atom is positioned closer to the interior $Cu^{2+}$ ion of the Cu paddlewheel. The close distance between the amide oxygen atom and the interior $Cu^{2+}$ ion, as seen in this configuration, is required for stabilizing a favorable interaction between the hydrogen molecules and the interior $Cu^{2+}$ ion.

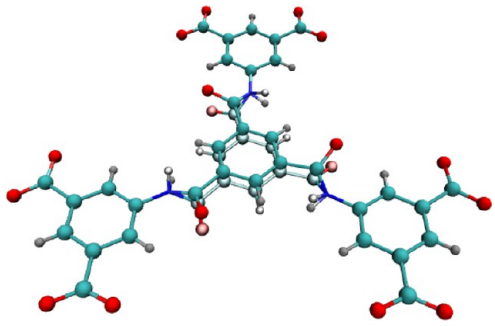

**Figure 2.** TPBTM linker showing the two configurations (A and B) of Cu-TPBTM. The glossy atoms correspond to configuration B. Atom colors: C = cyan, H = white, N = blue, O = red.

The crystal structure of as-synthesized Cu-TPBTM was also taken at 100 K. At this colder temperature, the MOF was also observed in two different configurations. One of the configurations, denoted herein as configuration C, had a similar amide oxygen atom orientation as configuration A, although it had a different puckering of the central aromatic ring of the linker. The other, denoted configuration D, can be characterized with the same displacement of the central aromatic ring as configuration A, but with a different amide oxygen atom orientation, similar to that observed in configuration B. Moreover, the crystal structure of Cu-TPBTM is slightly contracted at lower temperatures compared to the room temperature structure, with a unit cell length of 42.075 Å. This diminution of scale does not lead to favorable electrostatics that are required for the observed sorbate uptake in this MOF. Thus, the modeling results in configurations C and D are not shown. More details on these two configurations are provided later in the text and in the Supporting Information.

For the purpose of simulation, the MOF-$H_2$ interaction energy was decomposed into three components: repulsion/dispersion, permanant electrostatics, and polarization effects. These were modeled by the Lennard-Jones 12−6 potential, partial charges with Ewald summation,[26] and Thole-Applequist many-body polarization,[27,28] respectively. Note, long-range corrections were applied to all terms of the potential due to the finite size of the simulation box. The long-range contribution to the Lennard-Jones potential was implemented using a previously reported procedure.[29] Long-range electrostatic interactions was handled by performing full Ewald summation, and long-range polarization was implemented using the shifted-field formula according to Wolf et al.[30] Intramolecular interactions for both the framework and the


dx.doi.org/10.1021/jp402304a | J. Phys. Chem. C 2013, 117, 9340−9354

hydrogen potentials were constrained to rigid internal geometries. The total potential energy, $U$, for the system is described by

$$U = U_{rd} + U_{es} + U_{pol} \quad (1)$$

where $U_{rd}$, $U_{es}$, and $U_{pol}$ are the repulsion/dispersion, electrostatic, and polarization energy contributions, respectively. For the simulations at low temperatures (e.g., 77 K), quantum corrections were implemented through the fourth order Feynman-Hibbs correction according to the following equation:[31]

$$U_{FH} = \frac{\beta\hbar^2}{24\mu}\left(U'' + \frac{2}{r}U'\right) + \frac{\beta^2\hbar^4}{1152\mu^2}\left(\frac{15}{r^3}U' + \frac{4}{r}U''' + U''''\right) \quad (2)$$

where $\beta$ represents the quantity $1/kT$ ($T$ is the temperature, and $k$ is the Boltzmann constant), $\hbar$ is the reduced Planck's constant, $\mu$ represents the chemical potential of the reservoir, which was determined through the BACK equation of state,[32] and the primes indicate differentiation with respect to pair separation $r$.

For both configurations A and B of Cu-TPBTM, the atomic parameters for repulsion/dispersion interactions were provided by the Universal Force Field,[33] which has been shown to produce good results in MOF-sorbate studies in general[34−39] and *rht*-MOFs in particular.[20,40] The values for the Lennard-Jones parameters used in this study can be found in the Supporting Information.

Charge-quadrupole interactions were parametrized by point partial charges localized on the atomic positions. Twenty-four atoms in chemically distinct environments were identified within the Cu-TPBTM unit cell (Figure 3). A series of

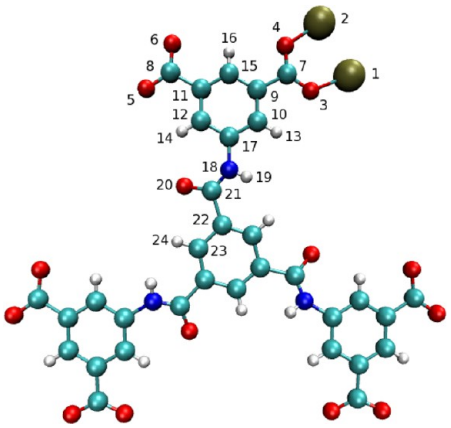


**Figure 3.** Chemically distinct atoms in Cu-TPBTM defining the numbering system corresponding to Table 1. Atom colors: C = cyan, H = white, N = blue, O = red, Cu = tan.

representational fragments were selected to examine these atoms in environments chemically similar to the MOF conditions. Chemical termination of fragments was achieved by the addition of hydrogen atoms as needed. Note, the two $Cu^{2+}$ ions that are part of the metal paddlewheel are indeed chemically distinct, as the carboxylate carbon−aromatic carbon bond (the bond between atoms 7 and 9 in Figure 3) cannot rotate freely in the MOF. Previous simulation studies on *rht*-MOFs[40,41] did not treat these ions as chemically distinct in their force field. Rather, these studies treated these chemically inequivalent $Cu^{2+}$ ions to be identical, with the same partial charge. The two $Cu^{2+}$ ions in *rht*-MOFs are in chemically distinguishable environments and if they are not treated as so within the force field, it can lead to inaccurate or difficult to interpret results.

The MOF partial charges were derived from the electrostatic potential surface of gas phase fragments using a least-squares fit approach[42−44] to localize charges on the atomic positions that are capable of reproducing the potential at a large number of points along the surface. For this, Hartree−Fock calculations were implemented using the NWChem *ab initio* simulation software.[45] The 6-31G* basis set was used for all first and second row atoms, as the overpolarization of gas phase fragments produced by this basis has been shown to conveniently produce values leading to the inclusion of effective polarization effects from condensed phase media.[46] The $Cu^{2+}$ ions were treated with the LANL2[47−49] double-$\zeta$ effective core potential basis set; this basis set was used to effectively describe the nucleus of many-electron atoms for previous MOF−sorbate simulation studies.[37,40]

Comparison of the resultant partial charges between candidate fragments for chemically isolated atoms, neglecting terminal atoms, exibited an unusually high degree of variation. Note, it is generally possible to derive partial charges from the electronic structure of the full crystal structure, but the large unit cell of *rht*-MOFs makes this computationally prohibitive.[44,50] Further, constructing representative fragments can lead to useful chemical insights into MOF electonics as it did in this case. Most notably, the $Cu^{2+}$ ions, labeled atoms 1 and 2 in Figure 3, alternated charges with the former having the higher charge in many fragments and the latter dominating in the rest. In situations where two or more Cu paddlewheels were included in the fragment, both cases often occurred simultaneously if like atoms were not constrained to equality. Further extensive examination of a large number of fragments yielded the origin of the deviation; a representative fragment is shown in Figure 4 and the remaining are in the Supporting Information. It was discovered that the presence of the amide group causes the interior $Cu^{2+}$ ion to increase in charge while the charge of the exterior $Cu^{2+}$ ion diminished. This charge flip, however, is only observed if the carbonyl oxygen atom is on the same side as the Cu paddlewheel (Figure 4). Otherwise, the charge of the interior $Cu^{2+}$ ion does not increase. Comparison

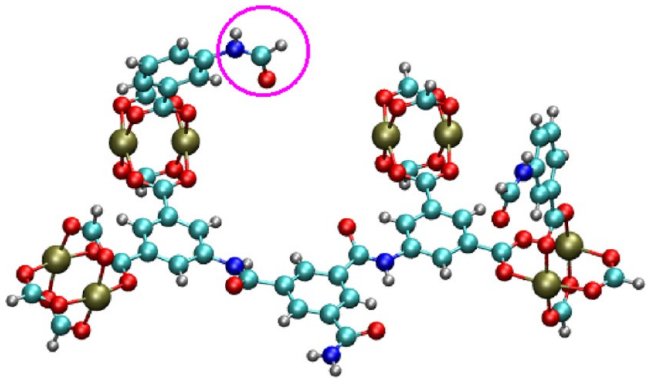

**Figure 4.** Example of a fragment of Cu-TPBTM that exhibits a higher charge magnitude on the interior $Cu^{2+}$ ion (atom label 1 in Figure 3) through electronic structure calculations. The circled functional group provides the proximal amide functionality required for the proper charge distribution about the chemically distinct $Cu^{2+}$ ions. Atom colors: C = cyan, H = white, N = blue, O = red, Cu = tan.


dx.doi.org/10.1021/jp402304a | J. Phys. Chem. C 2013, 117, 9340−9354

of fragments with the amide oxygen atoms in position for all $Cu^{2+}$ ions produced excellent agreement among charges in a number of fragments for both configurations A and B of Cu-TPBTM. The partial charges used in GCMC simulations for the chemically distinct atoms in both configurations of Cu-TPBTM are listed in Table 1. Most of the disparity in the partial charges between the two configurations lies between the atoms found within the amide group and the central ring of the linker.

**Table 1. Comparison of Partial Charges between Configurations A and B in Cu-TPBTM[a]**

| atom | label | A $q$ ($e^-$) | B $q$ ($e^-$) |
|---|---|---|---|
| Cu | 1 | 1.2292 | 1.1809 |
| Cu | 2 | 0.9902 | 1.0033 |
| O | 3 | −0.7320 | −0.7230 |
| O | 4 | −0.7445 | −0.7248 |
| O | 5 | −0.7234 | −0.7581 |
| O | 6 | −0.7590 | −0.7338 |
| C | 7 | 0.9687 | 0.9103 |
| C | 8 | 0.9837 | 0.9658 |
| C | 9 | −0.1884 | −0.3377 |
| C | 10 | −0.1542 | −0.0173 |
| C | 11 | −0.0947 | −0.2241 |
| C | 12 | −0.1732 | −0.1032 |
| H | 13 | 0.2136 | 0.2334 |
| H | 14 | 0.1923 | 0.2567 |
| C | 15 | −0.0706 | −0.1869 |
| H | 16 | 0.1994 | 0.2183 |
| C | 17 | 0.1497 | 0.3603 |
| N | 18 | −0.1989 | −0.6116 |
| H | 19 | 0.2098 | 0.3097 |
| O | 20 | −0.6582 | −0.6607 |
| C | 21 | 0.4696 | 0.8546 |
| C | 22 | 0.0916 | −0.3441 |
| C | 23 | −0.2630 | 0.1413 |
| H | 24 | 0.1720 | 0.0828 |

[a]Label of atoms corresponds to Figure 3.

In addition to emphasizing the importance of evaluating multiple fragments for partial charge determination, the dependency of the copper charges in the presence of the oxygen atom of the amide suggests the possibility of a distinct $H_2$ sorption mechanism in Cu-TPBTM as compared to PCN-61. Note, in PCN-61, the electronic structure calculations on a variety of fragments showed that the exterior $Cu^{2+}$ ion exhibited the higher positive charge of the two copper ions.[20] In Cu-TPBTM, the presence of the amide functional group causes the electrostatics of the $Cu^{2+}$ ions to change, as the interior $Cu^{2+}$ ion becomes the more positively charged species in this MOF.

In the previous work on PCN-61,[20] all electronic structure calculations on the molecular fragments of PCN-61 was performed using the 6-31G* basis set for all species, including the $Cu^{2+}$ ions. The partial charges for the chemically distinct atoms in PCN-61 were determined again using the LANL2DZ ECP basis set for the $Cu^{2+}$ ions while treating all other atoms at the 6-31G* level. This was done in order to provide a definite comparison to the results obtained in Cu-TPBTM. The partial charges that were calculated for PCN-61 using this scheme were comparable to ones calculated previously, although the magnitudes of the charges of the $Cu^{2+}$ ions decreased (see Table S9, Supporting Information). However, the difference in magnitudes between the charges of the two $Cu^{2+}$ ions were similar. Simulation of hydrogen sorption was performed on PCN-61 using the new set of charges at a few state points for only the polarizable model. The uptakes, the initial $Q_{st}$, the radial distribution functions, and the three-dimensional histograms for this model were functionally indistinguishable from that reported in the previous work (see Supporting Information).

Many-body polarization effects were parametrized by atomic point polarizabilities fit to a Thole-Applequist type model.[27,28,51] A brief overview is given in the Supporting Information. The atomic point polarizabilities for first and second row elements used a set of carefully parametrized empirical values that were shown to be highly transferable.[20,27,37,39,51−53] Thus, these atoms were given the exponential polarizabilities and associated damping parameter provided by the work of van Duijnen et al.[51] The $Cu^{2+}$ parameter was determined in previous work and produced excellent results in simulations of PCN-61.[20] The values for the atomic point polarizabilities used in this study can be found in the Supporting Information. Note, in our simulations, the MOF partial charges are overpolarized so no self-polarization is permitted.[20]

**B. Hydrogen Potentials.** Three hydrogen potential energy functions of increasing chemical accuracy were used in order to illustrate the essential physical interactions and associated potential energy terms required for accurate modeling of the

**Table 2. Parameters Used to Characterize the Buch, BSS, and BSSP Models[a]**

| model | site | $r$ (Å) | $\varepsilon$ (K) | $\sigma$ (Å) | $q$ ($e^-$) | $\alpha^\circ$ (Å$^3$) |
|---|---|---|---|---|---|---|
| Buch | H2G | 0.00000 | 34.20000 | 2.96000 | 0.0000 | 0.00000 |
| BSS | H2G | 0.00000 | 8.85160 | 3.22930 | −0.7464 | 0.00000 |
| | H2E | −0.37100 | 0.00000 | 0.00000 | 0.3732 | 0.00000 |
| | H2E | 0.37100 | 0.00000 | 0.00000 | 0.3732 | 0.00000 |
| | H2N | −0.32900 | 4.06590 | 2.34060 | 0.0000 | 0.00000 |
| | H2N | 0.32900 | 4.06590 | 2.34060 | 0.0000 | 0.00000 |
| BSSP | H2G | 0.00000 | 12.76532 | 3.15528 | −0.7464 | 0.69380 |
| | H2E | −0.37100 | 0.00000 | 0.00000 | 0.3732 | 0.00044 |
| | H2E | 0.37100 | 0.00000 | 0.00000 | 0.3732 | 0.00044 |
| | H2N | −0.36300 | 2.16726 | 2.37031 | 0.0000 | 0.00000 |
| | H2N | 0.36300 | 2.16726 | 2.37031 | 0.0000 | 0.00000 |

[a]H2G corresponds to the center-of-mass (median) site, H2E corresponds to the true atomic locations, and H2N corresponds to the Lennard-Jones off-site.


dx.doi.org/10.1021/jp402304a | J. Phys. Chem. C 2013, 117, 9340−9354

hydrogen sorption mechanism in Cu-TPBTM. Thus, these hydrogen potentials were used to assess the importance of van der Waals repulsion/dispersion, charge-quadrupole, and many-body polarization interactions in the simulation of hydrogen sorption in a heterogeneous environment such as a charged/polar MOF. The parameters for all three hydrogen potentials can be found in Table 2.

The first, here designated Buch,[21] is a single site model that includes only explicit repulsive/dispersive interaction terms with all other contributions implicitly approximated in a mean field fashion. While effective for bulk simulations, in heterogeneous (charged and polarizable) materials, where sorption mechanisms have greater dependency on electrostatic interactions, undersorption is typically observed.[20] It is used herein as a control model.

The Belof Stern Space (BSS) model[22] includes explicit repulsion/dispersion and charge-quadrupole interaction parameters, with the latter on the atomic and median positions and the former on the median and sites localized 0.329 Å from the center extending along the $C_\infty$ axis. Polarization is included as an implicit effect through capturing pair energetics in the gas phase, and this model reproduces bulk hydrogen data as well as accurate sorption in nonpolar MOFs.[22,38] Sorption in charged/polar MOFs using this model, however, is not well represented, as this model fails to describe the correct sorbate interactions in MOFs with open metal sites.[20]

The Belof Stern Space Polar (BSSP) model[22] is an analogue of the BSS model with explict atomic point polarizabilities on the atomic and median positions. In this model, the off-site Lennard-Jones parameters shift out to 0.363 Å from the median. This model has produced resonable results for bulk (including dense, high pressure) hydrogen and sorption in both nonpolar and polar MOFs.[20,22,37]

**C. Grand Canonical Monte Carlo.** Hydrogen sorption in Cu-TPBTM at 77 K, 87 K, and 298 K was simulated using GCMC methods, implemented in the Massively Parallel Monte Carlo (MPMC) code,[54] an in-house code that is used in our research group and is now available for download on Google Code. Periodic boundary conditions were applied in order to approximate an infinitely extended periodic lattice.

The average particle number was calculated via the grand canonical ensemble using the following expression:[55,56]

$$\langle N\rangle = \frac{1}{\Xi}\sum_{N=0}^{\infty} e^{\beta\mu N}\{\prod_{i=1}^{3N}\int_{-\infty}^{\infty} \mathrm{d}x_i\} N e^{-\beta U_{\mathrm{FH}}(x_1,\ldots x_{3N})} \quad (3)$$

where $\Xi$ is the grand canonical partition function, and $\beta$, $\mu$, and $U_{\mathrm{FH}}$ are terms that were defined earlier. For the simulations at 298 K, $U_{\mathrm{FH}}$ was replaced by $U$, as Feynman-Hibbs correction to the potential energy was not needed at this temperature.

The absolute weight percent of $H_2$ sorbed in the MOF is calculated by:

$$\mathrm{wt\%} = \frac{\langle N\rangle m}{M + \langle N\rangle m} \quad (4)$$

where $m$ is the molar mass of the sorbate and $M$ is the molar mass of the MOF.

The isosteric heat of adsorption, $Q_{st}$, were calculated from fluctuations of the number of particles and potential energy via:[57]

$$Q_{\mathrm{st}} = -\frac{\langle NU\rangle - \langle N\rangle\langle U\rangle}{\langle N^2\rangle - \langle N\rangle^2} + kT \quad (5)$$

Equation 5 is useful for model validation and these values are compared directly to $Q_{st}$ values that were calculated from experimental isotherms using the virial method.[58]

## III. RESULTS AND DISCUSSION

**A. Isotherms and Isosteric Heats of Adsorption.** The GCMC simulated low-pressure absolute hydrogen sorption isotherms for the three hydrogen potentials (Buch, BSS, and BSSP) in both considered configurations (A and B) of Cu-TPBTM at 77 K are plotted in Figure 5a and compared to experimental data. Note, the unit of wt% used here is defined as: (mass of $H_2$)/(mass of MOF + mass of $H_2$) × 100%. Not suprisingly, hydrogen sorption via the Buch model shows significant undersorption compared to the experimental data in both configurations of Cu-TPBTM at all state points considered. At 1.0 atm, the Buch model undersorbs the experimental isotherm by approximately 28% in both configurations. This demonstrates that simple van der Waals interaction is not sufficient to model hydrogen sorption in Cu-TPBTM effectively due to the heterogeneous environment of the framework. The Buch model agreement for the hydrogen uptakes in the crystal structures of both configurations indicates that alterations in pore dimensions and steric hindrances introduced through structural changes have a negligible effect on strictly van der Waals mechanisms in this MOF.

The BSS model shows an increase in hydrogen uptake in the framework compared to the Buch model for both configurations. This demonstrates that charge-quadrupole interactions are making an important contribution to the sorption mechanism. However, even with the addition of charge−quadrupole interactions, the isotherm for the BSS model falls short of the experimental isotherm. This result is consistent with the expectation that explicit polarization is requred for accurate interaction mechanisms with highly charged heterogeneous media in general and open-metal sites in particular.[20,37] The BSS model undersorbs the experimental data by approximately 9.0% at 1.0 atm for configuration A. However, a modest difference is observed for the BSS sorption results in configuration B, as simulations in this configuration produced an uptake that is approximately 0.20 wt % less than configuration A. This can be attributed to the significant differences between the Coulombic partial charges for both configurations (see Table 1).

When the BSSP model was simulated in both configurations of Cu-TPBTM, the sorption results for the two configurations were very different, with configuration A sorbing a significant quantity greater than configuration B at all state points. In addition, comparison of the BSSP isotherm with the experimental isotherm showed that the isotherm produced by this model is in excellent agreement with the experimental data; they are equivalent to within joint uncertainties. The maximum calculated error for the BSSP model is ±0.03 wt %.

On the other hand, it can be seen in the low-pressure sorption isotherm at 77 K that the BSSP model significantly undersorbs the experimental isotherm at all state points considered for simulation in configuration B. Moreover, the BSSP model isotherm is only slightly higher than the BSS model isotherm in configuration B, and it slightly undersorb the BSS model results in configuration A. This indicates that many-body polarization effects are contributing negligibly to the sorption structure for hydrogen sorption in this configuration. Putting it another way, only configuration A with the polar BSSP model results in sorption onto the open-metal sites at low


dx.doi.org/10.1021/jp402304a | J. Phys. Chem. C 2013, 117, 9340−9354

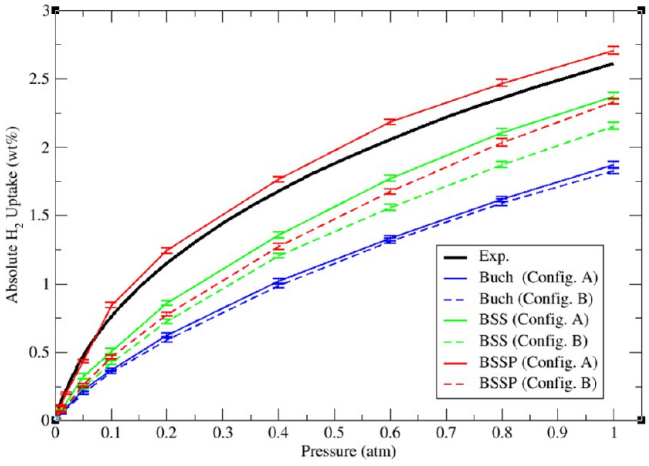


(a)

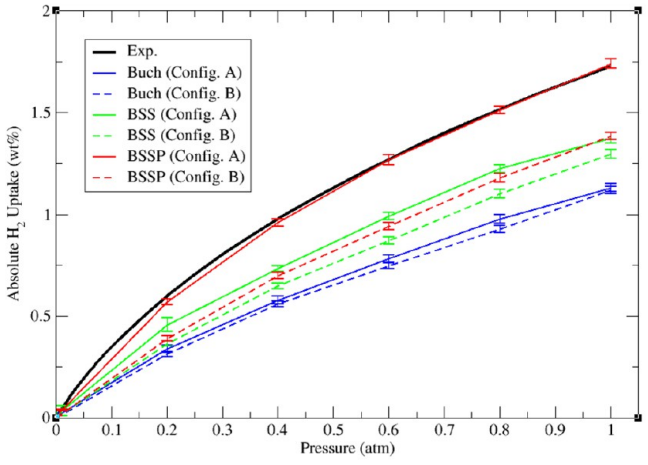


(b)

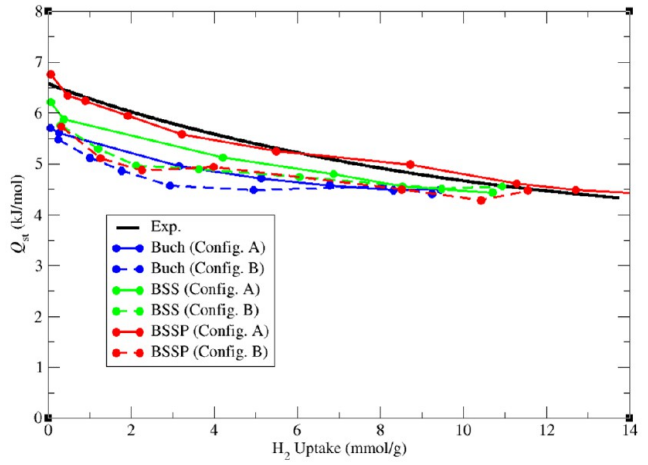


(c)

**Figure 5.** Low-pressure (up to 1.0 atm) absolute hydrogen sorption isotherms in Cu-TPBTM at (a) 77 K and (b) 87 K for experiment (black), Buch model (blue), BSS model (green), and BSSP model (red). (c) Isosteric heats of adsorption, $Q_{st}$, for hydrogen in Cu-TPBTM plotted against hydrogen uptakes corresponding to pressures between 0 and 1.0 atm at 77 K. Line type indicate the configuration of Cu-TPBTM in which the simulation was performed in, with solid corresponding to configuration A and dashed corresponding to configuration B.

pressures and outstanding agreement with experimental sorption across the entire low-pressure pressure range. From this, it is suggested that the addition of the sorbate causes the Cu-TPBTM crystal to shift into the more sorption-favored configuration similar to configuration A leading to the observed uptake.

This result is corroborated by data at 87 K where analogous trends for the simulated sorption isotherms for the three hydrogen potentials in both configurations can be seen (Figure 5b). The BSSP model in configuration A is in quantitative agreement with the experimental data; the other two models undersorb for only configuration A. All models undersorb for configuration B and demonstate increasing deviation from the configuration A results as more realistic potential energy terms are included in the $H_2$ potential. Note, the sorption results in configuration A are consistent to what was seen for the simulated hydrogen sorption isotherms in PCN-61 where induction effects also played a critical role in hydrogen sorption.[20] The simulations were also performed at 298 K, and these results are discussed below.

To probe the origin of the favorable sorption characterisitics of configuration A, a series of computational experiments were performed. Specifically, control simulations were performed using the BSSP model in configuration B where each chemically distinct atom was articifically assigned the point charges that were determined for the corresponding atoms in configuration A, and vice versa. For simulations in configuration B using the charges derived for configuration A, a marked increase in uptake was observed, though the isotherm still undersorbed the experimental results at 77 K and all pressures. For simulations in configuration A using the configuration B charges, a notable decrease in uptake at 1.0 atm was observed, while sorption in the low-pressure regime continued to duplicate experimental results. The latter finding indicates that the physical open-metal site sorption mechanisms were still observed in configuration A. From this, it can be established that the decreased uptake for configuration B is due to both steric effects and less favorable electrostatic interactions in this configuration. More details about these control simulations are included in the Supporting Information.

Although the hydrogen uptake for the BSSP model in configuration A is greater than the uptakes for the same model in configuration B in the low-pressure region, it was observed that the hydrogen uptakes for both configurations are nearly equivalent at higher pressures approaching saturation at about 30 atm − analgous to what was seen in PCN-61. This is true for the Buch and BSS models as well, with the uptakes being similar to those produced by the BSSP model. That is, all models in both configurations will have isotherms that converge at the saturation pressure where the MOF's detailed chemistry is less important. The observation that both configurations of Cu-TPBTM have nearly the same maximum sorption capacity was verified by calculating the pore volumes of the respective configurations using a previously reported modeling procedure involving helium; the data and the associated parameters are given in the Supporting Information.[59,60] Note, all three hydrogen potentials were also able to reproduce the experimental high pressure isotherm in PCN-61.[20] In both configurations at higher pressures, all models are essentially capturing the gross packing properties of the sorbed hydrogen in the MOF, as the MOF acts like a simple container at these pressures. Furthermore, like in PCN-61, it was observed that the isothermal compressibility,[57] $\beta_T$, decreases


dx.doi.org/10.1021/jp402304a | J. Phys. Chem. C 2013, 117, 9340−9354

rapidly as a function of pressure for all three models in both configurations of Cu-TPBTM. Moreover, the $\beta_T$ values decreases to a value that is characteristic of condensed hydrogen[61−64] when the hydrogen uptake in the structure begins to saturate.

The GCMC calculated isosteric heat of adsorption, $Q_{st}$, values for the three hydrogen potentials in both configurations of Cu-TPBTM are shown in Figure 5c and compared to those obtained experimentally. The $Q_{st}$ values for the three hydrogen potentials were calculated according to eq 5. Note, details for calculating the experimental $Q_{st}$ values are provided in the Supporting Information. As shown in the figure, the $Q_{st}$ values for the Buch and BSS models underestimated the experimental data in both configurations, especially at low loading. When comparing the results between the different configurations, the $Q_{st}$ values for the Buch model are comparable for the two configurations, while those for the BSS model are higher in configuration A; this is consistent to what was seen in the simulated hydrogen sorption isotherms. As for the BSSP model, it can be seen that larger $Q_{st}$ values were produced for this polarizable model in configuration A compared to configuration B, indicating that the MOF-$H_2$ binding energy is greater in configuration A. In addition, the $Q_{st}$ values for the BSSP model in configuration A is in good agreement with the experimental $Q_{st}$ values, while the same model underestimates these values in configuration B. This further suggests that configuration A is more favorable for hydrogen sorption than configuration B and is the dominant configuration present during sorption.

The initial $Q_{st}$ of Cu-TPBTM is characteristic of strong physisorption onto the open-metal sites in the MOF with values of approximately 6.6 kJ mol$^{-1}$. This value steadily decreases as hydrogen uptake in the MOF increases. All three hydrogen potentials show this trend for their $Q_{st}$ data. However, only the BSSP model simulated in configuration A was able to predict the initial $Q_{st}$ for $H_2$ as determined by experimental measurements. These results demonstrate both the necessity to include induction effects in the modeling of charged/polar MOFs with open-metal sites to accurately describe the interactions between the $H_2$ molecules and the metal and the importance of simulating sorption in the correct crystal structure of the MOF to describe the most critical MOF−sorbate interaction. Note, only the GCMC calculated $Q_{st}$ values at 77 K are shown in the figure. The results for $Q_{st}$ at 77 and 87 K were found to be nearly identical to within uncertainties.

Figure 6 shows the experimental and predicted hydrogen sorption isotherms for all three hydrogen potentials in both configurations of Cu-TPBTM at 298 K and pressures up to 100 atm. These are conditions that are suitable for hydrogen-powered applications like automobile propulsion. It can be seen from the simulated sorption isotherms that the hydrogen uptake capacity in the MOF decreases significantly from 77 to 298 K for all models in both configurations, consistent with the isosteric heat of adsorption values at the lower temperatures. At 298 K, simulation of Cu-TPBTM leads to uptakes at about 1.4 to 1.5 wt % at 100 atm. This is well below the ultimate target that was set by the DOE for an on-board hydrogen storage system.[2] When comparing the simulated hydrogen sorption isotherms between the models under these conditions, it can be seen that all three models produce nearly the same uptake at high pressures. Moreover, the uptakes are comparable between both A and B configurations of Cu-TPBTM. The majority of hydrogen molecules can be seen sorbed into the spaceous truncated tetrahedral and truncated octahedral cages and, at higher loadings, the fraction of hydrogen molecules interacting with the open-metal sites is relatively small.

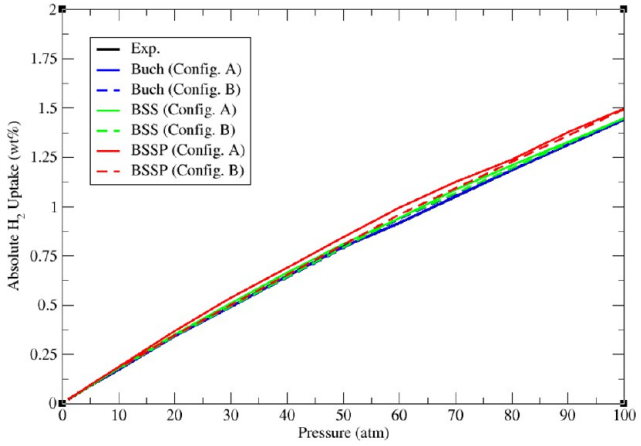


**Figure 6.** High-pressure (up to 100.0 atm) absolute hydrogen sorption isotherms in Cu-TPBTM at 298 K for experiment (black), Buch model (blue), BSS model (green), and BSSP model (red). Note, the simulated isotherms overlay the experimental isotherm. Line type indicate the configuration of Cu-TPBTM in which the simulation was performed in, with solid corresponding to configuration A and dashed corresponding to configuration B.

**B. Sorbate Radial Distribution Functions.** Figure 7a shows the radial distribution function, g($r$), between the center of mass of the sorbed hydrogen molecules and the interior $Cu^{2+}$ ion (labeled atom 1 in Figure 3) at 0.01 atm for all three hydrogen potentials in both configurations of Cu-TPBTM. The radial distribution functions show that the inclusion of many-body polarization strongly influences the structure of the sorbed hydrogen in the region of the copper ions in configuration A. In particular, the BSSP model shows that a large number of sorbed hydrogen molecules are approximately 2.5 Å apart from the interior $Cu^{2+}$ ion in this configuration. On the other hand, the 2.5 Å radial distribution peak in configuration B is much lower than that of configuration A. This peak corresponds to the loading of hydrogen onto the interior $Cu^{2+}$ ion of the open-metal sites. Hence, there is not a significant occupancy of hydrogen molecules about this site in configuration B. It can be inferred that the binding of hydrogen onto the interior $Cu^{2+}$ ion at low loadings is not as strong in configuration B. The initial $Q_{st}$ values that were calculated for the BSSP model in these two configurations support this notion well.

Note, the Buch and BSS models show that there are few sorbed hydrogen molecules within that distance from the interior copper ion in both configurations. This indicates that van der Waals interactions and charge-quadrupole effects do not contribute significantly to sorption at this site without the addition of induction effects. The majority of sorbed hydrogen molecules for the Buch and BSS models are about 6.0 Å apart from the interior $Cu^{2+}$ ion, which corresponds to sorption onto the corners of the truncated tetrahedral cages. Moreover, for configuration A, the radial distribution functions about the interior $Cu^{2+}$ ion for the Buch and BSS models are nearly identical while the one for BSSP is completely different, thus further demonstrating how many-body polarization can have an impact on the mechanism of hydrogen sorption in Cu-TPBTM.

The difference in the hydrogen/metal binding energy for the two configurations can be explained by the orientation of the


dx.doi.org/10.1021/jp402304a | J. Phys. Chem. C 2013, 117, 9340−9354

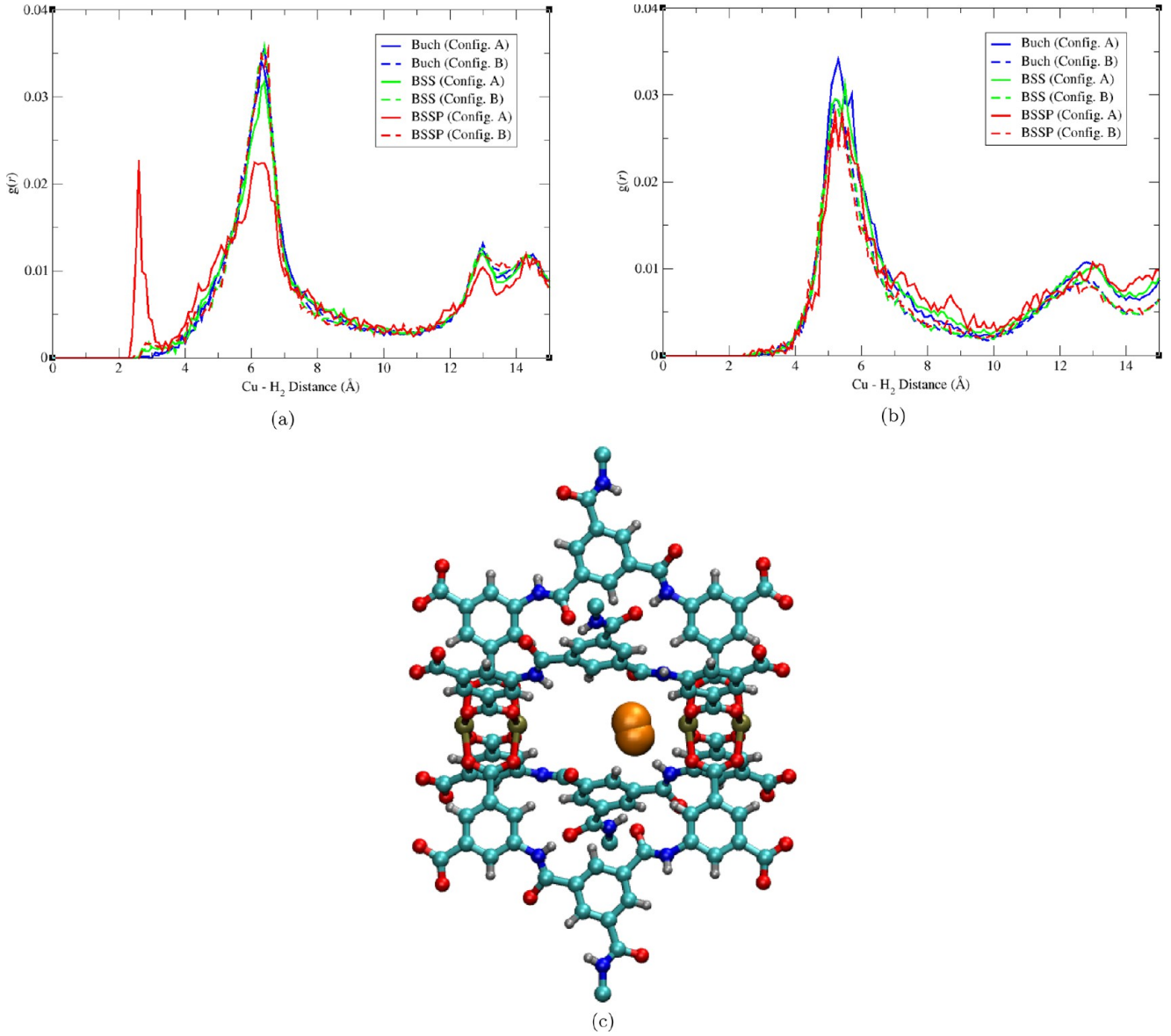


**Figure 7.** Radial distribution function about (a) the interior $Cu^{2+}$ ion (atom label 1 in Figure 3) and (b) the exterior $Cu^{2+}$ ion (atom label 2 in Figure 3) in Cu-TPBTM at 77 K and 0.01 atm for Buch model (blue), BSS model (green), and BSSP model (red). Line type indicate the configuration of Cu-TPBTM in which the simulation was performed in, with solid corresponding to configuration A and dashed corresponding to configuration B. (c) Molecular illustration of the T-shaped configuration between the BSSP model $H_2$ molecules (orange) and the interior $Cu^{2+}$ ion correlating to the 2.5 Å radial distribution peak seen for configuration A of Cu-TPBTM. Atom colors: C = cyan, H = white, N = blue, O = red, Cu = tan.

amide oxygen atom of the TPBTM linker in the respective configurations. The amide oxygen atom is responsible for causing the partial charge of the interior $Cu^{2+}$ ion to increase and directing hydrogen sorption onto the interior $Cu^{2+}$ ion of the open-metal site at initial loading. Because the interior $Cu^{2+}$ ion has the greater charge of the two $Cu^{2+}$ ions, it becomes the preferred metal site for hydrogen sorption. However, the interaction between the hydrogen molecules and the interior $Cu^{2+}$ ion is stabilized by the amide oxygen atom that is promixal to the interior $Cu^{2+}$ ion. In configuration A, the amide oxygen atom is more in line with the interior $Cu^{2+}$ ion with a Cu−O distance of 5.97 Å. Thus, in configuration A, there is a favorable interaction between the interior $Cu^{2+}$ ion and the hydrogen molecule as it sorbs onto the site at a distance of 2.5 Å away, and this hydrogen molecule makes a favorable interaction with the amide oxygen atom that is approximately 5.34 Å away. In configuration B, the amide oxygen atom is positioned away from the interior $Cu^{2+}$ ion with a Cu−O distance of 6.18 Å. Because the amide oxygen atom is oriented farther away from the interior $Cu^{2+}$ ion and the hydrogen molecule as it tries to sorb onto that site, the O atom cannot stabilize the interaction between the interior $Cu^{2+}$ ion and the hydrogen molecule as strongly as in configuration A. Thus, the hydrogen/metal interaction is weaker in configuration B due to the shifted position of the amide oxygen atom.

It is important to note that the occupancy of the hydrogen molecules about the open-metal sites in Cu-TPBTM contrasts what was observed in PCN-61. Previously, it was shown that the hydrogen molecules prefer to sorb onto the exterior $Cu^{2+}$ ion in PCN-61.[20] The BSSP hydrogen molecules were approximately 2.5 Å from the exterior $Cu^{2+}$ ion as shown in the radial distribution function in that work. This was due to the exterior $Cu^{2+}$ ion exhibiting a higher charge than the interior $Cu^{2+}$ ion in PCN-61 (1.7155 $e^-$ vs 1.0965 $e^-$). Note,


dx.doi.org/10.1021/jp402304a | J. Phys. Chem. C 2013, 117, 9340−9354

simulation of hydrogen sorption was also performed in PCN-61 where the $Cu^{2+}$ ions exhibited partial charges that were calculated using the LANL2DZ ECP basis set for the $Cu^{2+}$ ions. As in the previous study, the exterior $Cu^{2+}$ ion had the higher charge than the interior $Cu^{2+}$ ion (1.4362 $e^-$ vs 0.8660 $e^-$). The radial distrbution function about the exterior $Cu^{2+}$ ion for the BSSP model was similar to what was observed in the previous study (see Supporting Information). In Cu-TPBTM, the opposite was observed, as the interior $Cu^{2+}$ ion became the dominantly charged species over the exterior $Cu^{2+}$ ion (1.2292 $e^-$ vs 0.9902 $e^-$). This can be attributed to the presence of the O atom of the amide group in the linker, as the negatively charged oxygen causes the electrostatics of the $Cu^{2+}$ ions of the open-metal sites to change. Specifically, the charge of the exterior $Cu^{2+}$ ion in Cu-TPBTM decreases significantly relative to PCN-61. In addition, the radial distribution function about the exterior $Cu^{2+}$ ion in Cu-TPBTM is nearly the same for all models in both configurations (Figure 7b), suggesting that, even with many-body polarization interactions, the hydrogen molecules cannot sorb onto this site due to the lower charge of the exterior $Cu^{2+}$ ion. Likewise, it was observed that the radial distribution function about the interior $Cu^{2+}$ ion in PCN-61 is similar for all three hydrogen potentials (see Supporting Information).

As in PCN-61, the orientation of the BSSP hydrogen molecules about the open-metal sites in Cu-TPBTM is a T-shaped configuration (Figure 7c). This interaction between the BSSP hydrogen molecule and the interior $Cu^{2+}$ ion is similar to the Cu−$H_2$ interaction that was observed in HKUST-1 via inelastic neutron scattering and *ab initio* simulation studies.[65,66] These studies on HKUST-1 showed a similar T-shaped configuration between the hydrogen molecules and the $Cu^{2+}$ ion. Furthermore, a similar Cu−$H_2$ distance of 2.39 Å was observed in the studies on HKUST-1.

The 2.5 Å radial distribution peak for the BSSP model and the T-shaped configuration about the open-metal site in configuration A was only observed if the interior $Cu^{2+}$ ion had the higher charge of the two $Cu^{2+}$ ions in the force field for Cu-TPBTM. In order to verify this, fictitious control simulations of hydrogen sorption in configuration A of Cu-TPBTM were performed in cases where the exterior $Cu^{2+}$ ion had the higher charge (atom 2 in Figure 3 had a charge of 1.2292 $e^-$ whereas atom 1 had a charge of 0.9902 $e^-$) and where both $Cu^{2+}$ ions had the same charge (both had a charge of 1.1097 $e^-$). In both simulations, the hydrogen uptake capacity for the BSSP model at 1.0 atm were very similar to that of the normal case. However, when considering the uptakes at initial loading, the sorbed amounts for both control cases undersorbed the results for the normal force field. Examination of the radial distribution function about both the interior and exterior $Cu^{2+}$ ions for the control cases at 0.01 atm showed that sorption onto the open-metal site was not observed; this is indicated by the absence of the 2.5 Å radial distribution peak that was seen for the BSSP model about the interior $Cu^{2+}$ ion in configuration A of Cu-TPBTM (using the normal parametrized energy function) and in PCN-61 about the exterior $Cu^{2+}$ ion (Figure 8). Indeed, inspection of the modeled structure for the control simulations did not reveal any hydrogen molecules sorbing onto the open-metal sites. The majority of the molecules that were modeled given the hypothetical energy surface (including hydrogen molecules that were supposed to be occupying the interior $Cu^{2+}$ ion of the Cu paddlewheel in the normal force field) can be seen sorbing onto the sides and corners of the truncated tetrahedral cages.

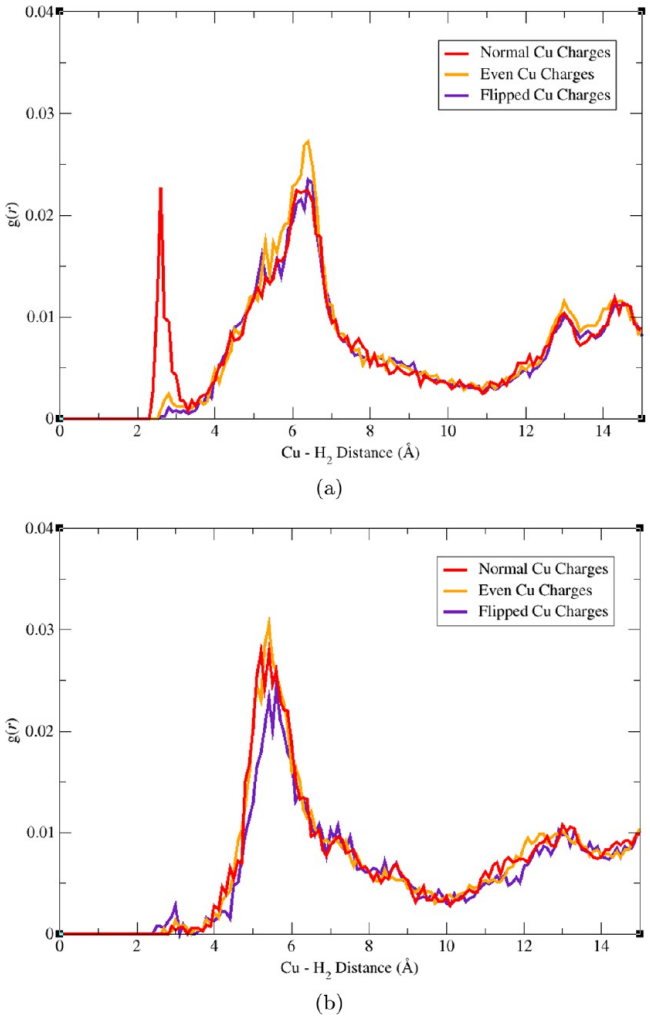


**Figure 8.** Radial distribution function about (a) the interior $Cu^{2+}$ ion (atom label 1 in Figure 3) and (b) the exterior $Cu^{2+}$ ion (atom label 2 in Figure 3) in configuration A of Cu-TPBTM at 77 K and 0.01 atm for the BSSP model in three situations describing the charges about the two $Cu^{2+}$ ions of the paddlewheel: the interior $Cu^{2+}$ ion having the higher charge (red); both $Cu^{2+}$ ions having the same charge (orange); and the exterior $Cu^{2+}$ ion having the higher charge (violet).

**C. Sorbate Induced Dipole Distributions.** The normalized dipole distribution for the BSSP model in configuration A of Cu-TPBTM at 77 K and various pressures (Figure 9) reveals three apparent dipolar hydrogen populations corresponding to the following induced dipole ranges: 0.20 D and above, 0.07 to 0.20 D, and 0.00 to 0.07 D. The dipole distribution for configuration A shows that a small number of hydrogen molecules have dipole magnitudes of 0.20 D and above. Correlating these dipole magnitudes to regions of occupancy inside Cu-TPBTM reveals that the hydrogen molecules with these dipoles sorb onto the interior $Cu^{2+}$ ion of the open metal site at initial loading (Figure 10a). This is expected given the highly charged interior $Cu^{2+}$ ion inducing higher dipoles on the hydrogen molecules, resulting in strong sorption. This also depends on the detailed interplay between sterics and permanant and induced electrosctatics, given that configuration B does not show a consistent binding to the open-metal sites. Thus, it seems that configuration A produces a "template" of


dx.doi.org/10.1021/jp402304a | J. Phys. Chem. C 2013, 117, 9340−9354

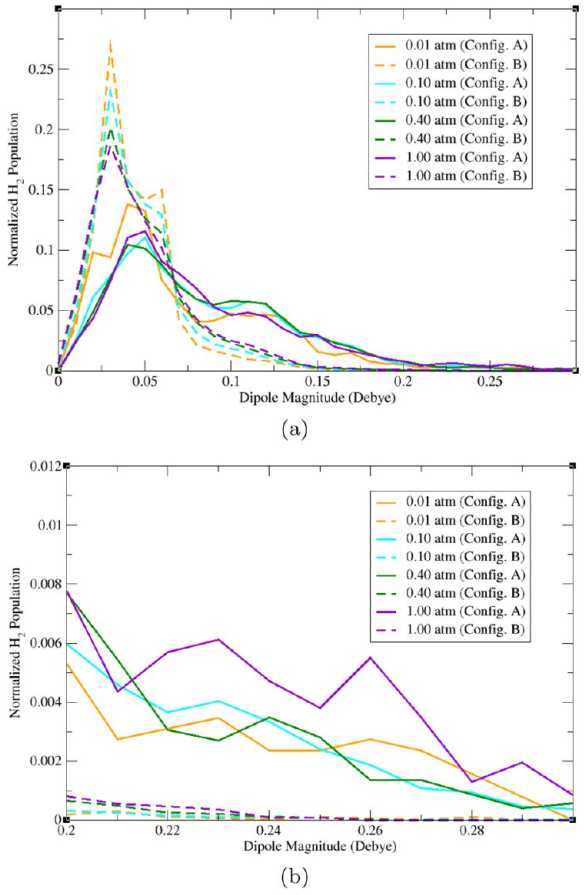


**Figure 9.** (a) Normalized hydrogen dipole distribution for the BSSP model at 77 K and various pressures for both configurations of Cu-TPBTM from 0.0 to 0.30 D. (b) Magnified region of the dipole distribution from 0.20 to 0.30 D.

ordered relatively strongly bound hydrogen molecules that leads to a consistently higher sorption for the entire low pressure range. This packing is aided by polarization (comparing BSS and BSSP hydrogen isosteric heats of adsorption via Figure 5c), and apparent steric efficiency compared to the more disordered hydrogen molecules in configuration B.

Note, this is distinct from the occupancy that was observed for the high dipolar species in PCN-61. In PCN-61, it was shown that the hydrogen molecules with the highest dipoles sorbed onto the exterior $Cu^{2+}$ ion at initial loading.[20] This is due to the fact that the exterior $Cu^{2+}$ ion in PCN-61 was the dominantly charged species of the two $Cu^{2+}$ ions, whereas the effect is reversed in Cu-TPBTM. Thus, a different sorption structure is observed in Cu-TPBTM with binding to different copper ions. In configuration B of Cu-TPBTM, there were almost no hydrogen molecules with dipole magnitudes of 0.20 D and above. Note, the changes associated with the environments provided by configuration A, PCN-61, and configuration B lead to binding to the interior, exterior, or neither copper ion, respectively. This suggests tunability of the metal binding sites even toward the chemically simple hydrogen molecule through reasonbly small configurational changes. The highest dipolar species at low loading in configuration B were sorbed onto the interior of the MOF with relatively weaker $H_2$-metal interactions; hydrogen is excluded from metal ion access because it lacks synergistic

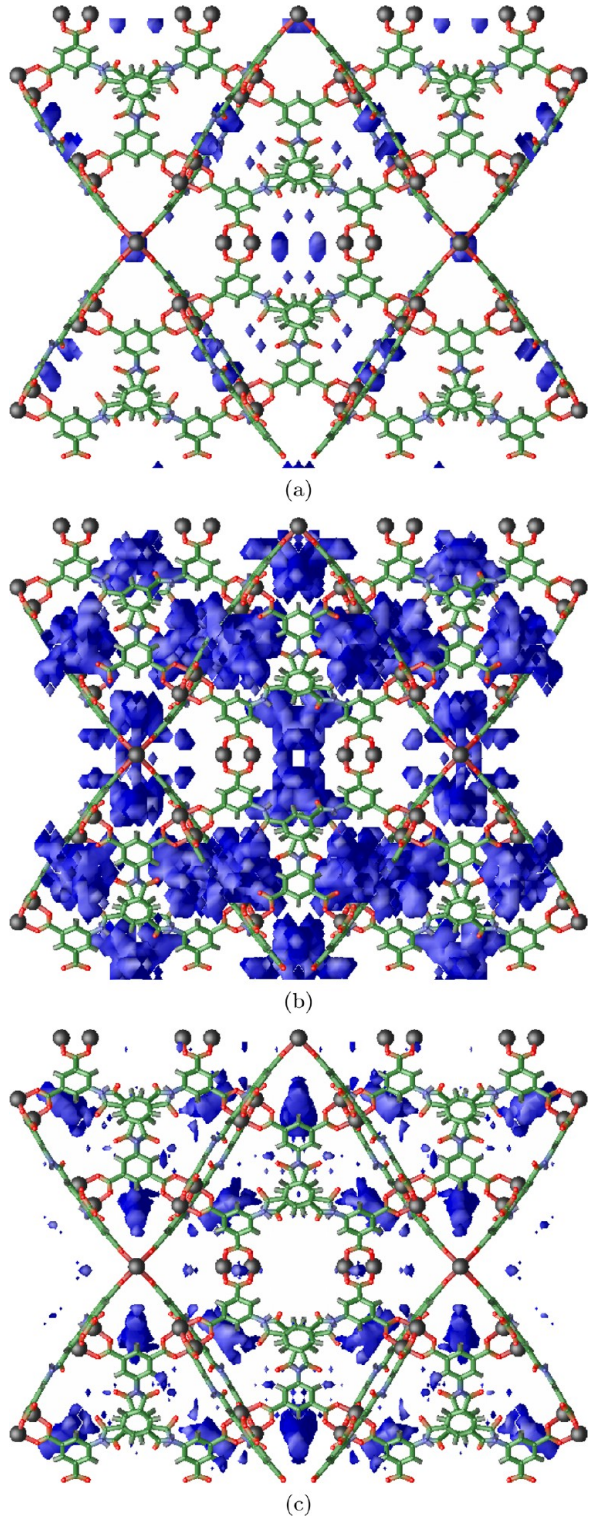


**Figure 10.** 3-D histograms of hydrogen sorption in Cu-TPBTM at 77 K and 0.01 atm showing the sites of hydrogen sorption (blue) for low loadings as a function of induced dipole magnitude: (a) 0.20 D and up, (b) 0.10 to 0.20 D, and (c) 0.00 to 0.10 D. Atom colors: C = green, H = white, N = blue, O = red, Cu = black.

interaction, present in configuration A, with the amide oxygen atom distal from the interior $Cu^{2+}$ ion in this configuration.

The dipole distribution shows that there is a broad peak from 0.07 to 0.20 D for configuration A, but that peak is diminished in configuration B. Examination of the 3-D histogram


dx.doi.org/10.1021/jp402304a | J. Phys. Chem. C 2013, 117, 9340−9354

correlating to dipole magnitudes of 0.07 to 0.20 D in configuration A (Figure 10b) shows that a large population of hydrogen molecules with these dipoles sorb onto the sides of the truncated tetrahedral cages. At the sides of these cages are the amide groups of the TPBTM linker; because amide functional groups increase hydrogen binding affinity, it is not surprising that the hydrogen molecules are found there. A closer look at this region of occupancy reveals that the hydrogen molecules sorbed onto those amide groups are in the region of the interior $Cu^{2+}$ ion. Thus, the secondary sorption site in this MOF can be seen as the hydrogen molecules in proximity of both the amide group and the interior $Cu^{2+}$ ion. The population of hydrogen molecules loading onto this site is reduced at all corresponding pressures in configuration B. This can be explained by the relatively unfavorable electrostatic interactions observed in configuration B. Specifically, the partial charge for the amide carbon atom is more positive in configuration B, and when it is combined with the charge for the associated amide O atom, the carbonyl group is net positive and it repels the hydrogen molecules from sorbing onto this site. The loading onto the sides of the truncated tetrahedron is rarely seen for configuration B across all state points, and this explains the dramatic difference in the simulated sorption isotherms for the BSSP model between both configurations as seen in Figure 5. At pressures near saturation, these sites become available for the hydrogen molecules in configuration B as the MOF acts essentially as a container at these conditions.

The low dipolar population, correlating to 0.00 to 0.07 D (Figure 10c), corresponds to hydrogen molecules can be seen occupying the corners of the truncated tetrahedral cages where it sorbs onto the vertices of the copper paddlewheels. These sorption sites are also seen for the Buch and BSS models. Moreover, this site corresponds to the 6.0 Å peak seen in the radial distribution function about the interior $Cu^{2+}$ ion for all three models in both configurations. This indicates that this site is dominated by van der Waals and charge-quadrupole interactions, whereas induction effects contribute slightly. For configuration B of Cu-TPBTM, a large number of hydrogen molecules were found sorbing in this region; this is the main site that the hydrogen molecules occupy in this configuration as the tendency of the hydrogen molecules to sorb onto the interior $Cu^{2+}$ ion and also the sides of the truncated tetrahedral cages at initial loading is extremely small. Note, in the control simulations where the partial charges on the $Cu^{2+}$ ions were equivalent or flipped relative to the normal force field, the hydrogen molecules with the highest dipoles were not seen sorbing onto the open-metal sites. Instead, they were seen sorbing onto the sides and corners of the truncated tetrahedral cages. Again, this suggests significant chemical tunability of metal binding sites.

**D. Effects from Variant Crystal Structures.** The crystal structure of Cu-TPBTM shows two possible configurations of the framework at room temperature. However, the theoretical sorption data strongly suggest that configuration A is dominant with $H_2$ sorbed at low temperatures, permitting favorable MOF-$H_2$ interactions and significantly increased loading compared to configuration B. Note, currently, an energy minimization of the Cu-TPBTM unit cell cannot be performed due to its large unit cell size, so the structure cannot be optimized to explore the sorbed MOF phase space.

Insights into the different configurations of Cu-TPBTM were obtained from the crystal structure of the MOF at both high and low temperatures. The crystal structure of Cu-TPBTM that was reported by Zheng et al. was taken at 293 K.[12] In this study, the Cu-TPBTM crystals were synthesized using the previously reported procedure,[12] and the single-crystal structure of the as-synthesized Cu-TPBTM crystals was taken at 100 K (see Supporting Information for more details). The cold crystal structure of the MOF also revealed two related configurations of the framework. One of the crystal arrangements (configuration C) corresponds to a configuration that has a similar orientation and distance between the interior $Cu^{2+}$ ion and the amide O atom as in configuration A, but with a different pucking of the central aromatic ring. The other configuration (configuration D) is very similar to configuration A, but the amide O atom is positioned a little farther away from the interior $Cu^{2+}$ ion. In addition, the MOF undergoes a slight contraction of approximately 0.08 Å in all dimensions at low temperatures.

Electronic structure calculations were performed on both of these cold temperature configurations of Cu-TPBTM. Fragments of similar type to those selected for configurations A and B were also used. However, the calculations on a variety of these fragments for both configurations showed significant differences in charges in comparison to the room temperature configurations, most notably the exterior $Cu^{2+}$ ion having the higher charge on the copper paddlewheel. This resulted in less favorable MOF−sorbate interactions for $H_2$ in Cu-TPBTM, which is consistent with earlier demonstration that the interior $Cu^{2+}$ ion must have the higher charge to capture the binding of hydrogen molecules onto the open-metal sites and reproduce experimental measurements. It is predicted that this phenomenon occurs due to the slight displacement of the atoms relative to the $Cu^{2+}$ ions as a result of the contraction; this is especially for those atoms in the amide group. Simulations of hydrogen sorption at 77 K using the BSSP model in both configurations C and D in their respective derived forced fields showed undersorption compared to the experimental isotherm. Thus, even though the experimental hydrogen sorption measurements were performed on the Cu-TPBTM crystal at low temperatures, our simulations cannot capture the correct sorption behavior in the cold temperature crystal structures. The earlier described results demonstrate that the MOF likely shifts to the ambient temperature configuration A crystal arrangement upon hydrogen sorption.

Note that although it is possible to treat the flexibility of the MOF during simulation,[67−69] such a task was not performed here due to computational expense, especially considering the large size of the Cu-TPBTM unit cell. For the simulations at low temperatures, constraining the MOF to be rigid during the simulation seems appropriate at 77 and 87 K since phonons are not thought to be important. In addition, crystallographic studies of Co-TPBTM,[12] the Co analogue of Cu-TPBTM, reveals that only configuration A exists for the Co variant, thus further suggesting that configuration A is the dominant configuration of the amide-based *rht* framework. Perhaps the other configurations are metastable kinetic phases of the copper containing MOF.

## IV. CONCLUSION

This study shows the importance of many-body polarization interactions in the modeling of hydrogen sorption in a highly polar MOF such as Cu-TPBTM. Polarization leads to significant sorbate ordering at low pressure that leads to higher sorption for the entire low pressure region below one atmosphere. It was also found that only one of the


dx.doi.org/10.1021/jp402304a | J. Phys. Chem. C 2013, 117, 9340−9354

experimentally observed configurations (configuration A) of the neat MOF crystal structure leads to sorption isotherms and isosteric heats of adsorption observed experimentally. Calculation of the MOF−$H_2$ binding energy for both configurations via the $Q_{st}$ demonstrates that configuration A has a maximum at low loading characteristic of $H_2$−copper ion interactions.[11,70] Distinct neat crystal structures at ambient and low temperatures were also examined for their sorption characteristics. It was demonstrated that seemingly small changes in MOF crystal configuration lead to different overall sorption and associated mechanisms.

It was further demonstrated that the presence of the amide functional groups in the TPBTM linker changed the electrostatics of the $Cu^{2+}$ ions of the paddlewheel relative to PCN-61. In PCN-61, the presence of a nonpolar alkyne group on the linker led to a higher relative charge on the exterior $Cu^{2+}$ ion in the MOF. In Cu-TPBTM, the presence of a polar amide group on the linker led to a higher charge on the interior $Cu^{2+}$ ion, thus reversing the electrostatics of the $Cu^{2+}$ ions. This can be explained by the presence of the oxygen atom of the amide group, as the negatively charged oxygen causes the interior $Cu^{2+}$ ion to exhibit a higher positive charge. Substituting a nonpolar linker with a polar linker changes the mechanism of hydrogen sorption. With the interior $Cu^{2+}$ ion having the higher charge of the two coppers ions, it becomes the preferred metal binding site for hydrogen sorption, which is contrast to what was observed in PCN-61. The results shown in this study suggest the possibility for experimentalists to tune which site they want the sorbate to bind to upon initial loading through aspirational chemical modifications of a MOF. In essence, changing one functional group in the organic linker leads to a different binding site for gas sorption; this allows for the flexibility to control desired binding sites. Computataional experiments, artificially modifying the copper ion charges, also showed significant tunability.

On the basis of the results observed previously for PCN-61[20] and in this study for Cu-TPBTM, the initial binding sites for other *rht*-MOFs can be predicted. For instance, in *rht*-MOF-1,[8] where the MOF is constructed using trigonal $Cu_3O$ trimers through 5-tetrazolylisophthalate moieties, one would expect the sorbate to bind onto the interior $Cu^{2+}$ ion for the metal paddlewheel sorption at low loading. This is because the electronegative nitrogen atoms on the tetrazolate moieties are proximal to the interior $Cu^{2+}$ ions and will cause this $Cu^{2+}$ ion to increase in charge through electronic structure calculations. As another example, in PCN-68,[11] which is similar to PCN-61 except that the central benzene ring of the linker is replaced by a 1,3,5-triphenylbenzene group, it would be expected that the exterior $Cu^{2+}$ ion will have the higher charge of the two $Cu^{2+}$ ions here. This MOF contains a highly nonpolar linker, and thus, it will not cause the interior $Cu^{2+}$ ion to exhibit a higher partial positive charge. It is deemed that the sorbate will load onto the exterior Cu ion in this MOF initially.

*rht*-MOFs are a very promising platform of MOFs that have been shown to exhibit high hydrogen uptake capacity due to their open-metal sites, tunability, small pore sizes, and high surface area.[11,12] Some variants were also shown to be water and acid stable.[41] As seen in this study, and as shown experimentally,[1,14,70−74] the presence of a polar functional group on the linker can enhance hydrogen uptake even further. The experimental hydrogen sorption studies have shown that Cu-TPBTM has a hydrogen uptake of 2.61 wt % at 77 K and 1.0 atm and an initial $Q_{st}$ value of 6.6 kJ/mol. However, these values fall short to those reported for an *rht*-MOF called Cu-TDPAT.[14,41,75] This MOF contains a 1,3,5-triazine group as the central aromatic ring of the linker, and the carbon atoms at the 2, 4, and 6 positions are connected to amine functional groups. This MOF was shown to have the highest hydrogen uptake of *rht*-MOFs synthesized thus far and will possibly be considered for computational investigations in the future.

The development of highly accurate and transferable anisotropic many-body potentials of other sorbates such as $CO_2$, $CH_4$, and $N_2$ is currently ongoing,[76] and utilization of these potentials to simulate sorption in *rht*-MOFs as well as other charged/polar MOFs is a task that will be investigated in the future. Based on the results of this study and the fact that the interior $Cu^{2+}$ ion has the higher positive charge of the two metal ions, it is predicted that the favorable site of $CO_2$ sorption in Cu-TPBTM would be between the interior $Cu^{2+}$ ions of adjacent paddlewheels where each oxygen atom of the $CO_2$ molecule coordinates to the interior $Cu^{2+}$ ion of respective paddlewheels. In addition, once the potentials of these sorbates have been developed, the selective separation of gas mixtures will be explored.

## ■ ASSOCIATED CONTENT

### Supporting Information

Details of experimental procedures and electronic structure calculations, tables of properties, pictures of MOF fragments, and additional content. This material is available free of charge via the Internet at http://pubs.acs.org.

## ■ AUTHOR INFORMATION

### Corresponding Author

*E-mail: brian.b.space@gmail.com.

### Author Contributions

‡Authors contributed equally

### Notes

The authors declare no competing financial interest.

## ■ ACKNOWLEDGMENTS

This work was supported by the National Science Foundation (Award No. CHE-1152362). Computations were performed under a XSEDE Grant (No. TG-DMR090028) to B.S. This publication is also based on work supported by Award No. FIC/2010/06, made by King Abdullah University of Science and Technology (KAUST). The authors also thank the Space Foundation (Basic and Applied Research) for partial support. The authors would like to acknowledge the use of the services provided by Research Computing at the University of South Florida. Lastly, the authors thank Professor Randy W. Larsen and his research group for interactive discussions on this project.

## ■ REFERENCES

(1) Collins, D. J.; Ma, S.; Zhou, H.-C. In *Hydrogen and Methane Storage in Metal-Organic Frameworks*; John Wiley & Sons, Inc.: New York, 2010; pp 249−266.

(2) *DOE Targets for Onboard Hydrogen Storage Systems for Light-Duty Vehicles*, http://www1.eere.energy.gov/hydrogenandfuelcells/storage/pdfs/targets_onboard_hydro_storage_explanation.pdf; Accessed November 16, 2011.

(3) Collins, D. J.; Zhou, H.-C. *J. Mater. Chem.* **2007**, *17*, 3154−3160.

(4) Suh, M. P.; Park, H. J.; Prasad, T. K.; Lim, D.-W. *Chem. Rev.* **2012**, *112*, 782−835.

(5) Liu, Y.; Eubank, J.; Cairns, A.; Eckert, J.; Kravtsov, V.; Luebke, R.; Eddaoudi, M. *Angew. Chem., Int. Ed.* **2007**, *46*, 3278−3283.
(6) Farha, O. K.; Yazaydin, A. O.; Eryazici, I.; Malliakas, C. D.; Hauser, B. G.; Kanatzidis, M. G.; Nguyen, S. T.; Snurr, R. Q.; Hupp, J. T. *Nat. Chem.* **2010**, *2*, 944−948.
(7) Eddaoudi, M.; Moler, D. B.; Li, H.; Chen, B.; Reineke, T. M.; O'Keeffe, M.; Yaghi, O. M. *Acc. Chem. Res.* **2001**, *34*, 319−330 PMID: 11308306..
(8) Nouar, F.; Eubank, J. F.; Bousquet, T.; Wojtas, L.; Zaworotko, M. J.; Eddaoudi, M. *J. Am. Chem. Soc.* **2008**, *130*, 1833−1835.
(9) Zou, Y.; Park, M.; Hong, S.; Lah, M. S. *Chem. Commun.* **2008**, 2340−2342.
(10) Zhao, D.; Yuan, D.; Sun, D.; Zhou, H.-C. *J. Am. Chem. Soc.* **2009**, *131*, 9186−9188.
(11) Yuan, D.; Zhao, D.; Sun, D.; Zhou, H.-C. *Angew. Chem.* **2010**, *122*, 5485−5489.
(12) Zheng, B.; Bai, J.; Duan, J.; Wojtas, L.; Zaworotko, M. J. *J. Am. Chem. Soc.* **2011**, *133*, 748−751.
(13) Yan, Y.; Yang, S.; Blake, A. J.; Lewis, W.; Poirier, E.; Barnett, S. A.; Champness, N. R.; Schroder, M. *Chem. Commun.* **2011**, *47*, 9995−9997.
(14) Li, B.; et al. *Angew. Chem., Int. Ed.* **2012**, *51*, 1412−1415.
(15) Eryazici, I.; Farha, O. K.; Hauser, B. G.; Yazaydin, A. O.; Sarjeant, A. A.; Nguyen, S. T.; Hupp, J. T. *Cryst. Growth Design* **2012**, *12*, 1075−1080.
(16) Zheng, B.; Yang, Z.; Bai, J.; Li, Y.; Li, S. *Chem. Commun.* **2012**, *48*, 7025−7027.
(17) Luebke, R.; Eubank, J. F.; Cairns, A. J.; Belmabkhout, Y.; Wojtas, L.; Eddaoudi, M. *Chem. Commun.* **2012**, *48*, 1455−1457.
(18) Eubank, J. F.; Nouar, F.; Luebke, R.; Cairns, A. J.; Wojtas, L.; Alkordi, M.; Bousquet, T.; Hight, M. R.; Eckert, J.; Embs, J. P.; Georgiev, P. A.; Eddaoudi, M. *Angew. Chem., Int. Ed.* **2012**, *51*, 10099−10103.
(19) Zhao, X.; Sun, D.; Yuan, S.; Feng, S.; Cao, R.; Yuan, D.; Wang, S.; Dou, J.; Sun, D. *Inorg. Chem.* **2012**, *51*, 10350−10355.
(20) Forrest, K. A.; Pham, T.; McLaughlin, K.; Belof, J. L.; Stern, A. C.; Zaworotko, M. J.; Space, B. *J. Phys. Chem. C* **2012**, *116*, 15538−15549.
(21) Buch, V. *J. Chem. Phys.* **1994**, *100*, 7610−7629.
(22) Belof, J. L.; Stern, A. C.; Space, B. *J. Chem. Theory Comput.* **2008**, *4*, 1332−1337.
(23) Mankoo, P. K.; Keyes, T. *J. Phys. Chem. B* **2006**, *110*, 25074−25079.
(24) Keyes, T.; Napoleon, R. L. *J. Phys. Chem. B* **2011**, *115*, 522−531.
(25) Nugent, P.; Belmabkhout, Y.; Burd, S. D.; Cairns, A. J.; Luebke, R.; Forrest, K.; Pham, T.; Ma, S.; Space, B.; Wojtas, L.; Eddaoudi, M.; Zaworotko, M. J. *Nature* **2013**, *495*, 80−84.
(26) Ewald, P. P. *Ann. Phys.* **1921**, *369*, 253−287.
(27) Applequist, J.; Carl, J. R.; Fung, K.-K. *J. Am. Chem. Soc.* **1972**, *94*, 2952−2960.
(28) Thole, B. *Chem. Phys.* **1981**, *59*, 341−350.
(29) Siperstein, F.; Myers, A.; Talu, O. *Mol. Phys.* **2002**, *100*, 2025−2030.
(30) Wolf, D.; Keblinski, P.; Phillpot, S. R.; Eggebrecht, J. *J. Chem. Phys.* **1999**, *110*, 8254.
(31) Feynman, R. P.; Hibbs, A. R. *Quantum Mechanics and Path Integrals*; McGraw-Hill: New York, 1965; Chapter 10, Sect. 3, p 281.
(32) Boublík, T. *Fluid Phase Equilib.* **2005**, *240*, 96−100.
(33) Rappé, A. K.; Casewit, C. J.; Colwell, K. S.; Goddard, W. A.; Skiff, W. M. *J. Am. Chem. Soc.* **1992**, *114*, 10024−10035.
(34) Kawakami, T.; Takamizawa, S.; Kitagawa, Y.; Maruta, T.; Mori, W.; Yamaguchi, K. *Polyhedron* **2001**, *20*, 1197−1206.
(35) Sagara, T.; Klassen, J.; Ganz, E. *J. Chem. Phys.* **2004**, *121*, 12543.
(36) Garberoglio, G.; Skoulidas, A. I.; Johnson, J. K. *J. Phys. Chem. B* **2005**, *109*, 13094−13103.
(37) Belof, J. L.; Stern, A. C.; Eddaoudi, M.; Space, B. *J. Am. Chem. Soc.* **2007**, *129*, 15202−15210.
(38) Belof, J. L.; Stern, A. C.; Space, B. *J. Phys. Chem. C* **2009**, *113*, 9316−9320.
(39) Stern, A. C.; Belof, J. L.; Space, B. *J. Chem. Phys.* **2012**, *136*, 034705.
(40) Babarao, R.; Eddaoudi, M.; Jiang, J. W. *Langmuir* **2010**, *26*, 11196−11203.
(41) Zhang, Z.; Li, Z.; Li, J. *Langmuir* **2012**, *28*, 12122−12133.
(42) Chirlian, L. E.; Francl, M. M. *J. Comput. Chem.* **1987**, *8*, 894−905.
(43) Breneman, C. M.; Wiberg, K. B. *J. Comput. Chem.* **1990**, *11*, 361−373.
(44) Chen, D.-L.; Stern, A. C.; Space, B.; Johnson, J. K. *J. Phys. Chem. A* **2010**, *114*, 10225−10233.
(45) Valiev, M.; Bylaska, E.; Govind, N.; Kowalski, K.; Straatsma, T.; Dam, H. V.; Wang, D.; Nieplocha, J.; Apra, E.; Windus, T.; de Jong, W. *Comput. Phys. Commun.* **2010**, *181*, 1477−1489.
(46) Cornell, W. D.; Cieplak, P.; Bayly, C. I.; Gould, I. R.; Merz, K. M.; Ferguson, D. M.; Spellmeyer, D. C.; Fox, T.; Caldwell, J. W.; Kollman, P. A. *J. Am. Chem. Soc.* **1995**, *117*, 5179−5197.
(47) Stevens, W. J.; Basch, H.; Krauss, M. *J. Chem. Phys.* **1984**, *81*, 6026.
(48) Hay, P. J.; Wadt, W. R. *J. Chem. Phys.* **1985**, *82*, 270.
(49) LaJohn, L. A.; Christiansen, P. A.; Ross, R. B.; Atashroo, T.; Ermler, W. C. *J. Chem. Phys.* **1987**, *87*, 2812.
(50) Campañá, C.; Mussard, B.; Woo, T. K. *J. Chem. Theory Comput.* **2009**, *5*, 2866−2878.
(51) van Duijnen, P. T.; Swart, M. *J. Phys. Chem. A* **1998**, *102*, 2399−2407.
(52) DeVane, R.; Space, B.; Perry, A.; Neipert, C.; Ridley, C.; Keyes, T. *J. Chem. Phys.* **2004**, *121*, 3688−3701.
(53) Perry, A.; Neipert, C.; Space, B.; Moore, P. B. *Chem. Rev.* **2006**, *106*, 1234−1258.
(54) Belof, J. L.; Space, B. *Massively Parallel Monte Carlo (MPMC)*, Available on Google Code.
(55) McQuarrie, D. A. *Statistical Mechanics*; University Science Books: Sausalito, CA, 2000; Chapter 3, p 53.
(56) Frenkel, D.; Smit, B. *Understanding Molecular Simulation: From Algorithms to Applications*; Academic Press: New York, 2002; Chapter 5, Sect. 6.1, p 129.
(57) Nicholson, D.; Parsonage, N. G. *Computer Simulation and the Statistical Mechanics of Adsorption*; Academic Press: London, 1982; Chapter 3, Sect. 4, p 97.
(58) Dinca, M.; Dailly, A.; Liu, Y.; Brown, C. M.; Neumann, D. A.; Long, J. R. *J. Am. Chem. Soc.* **2006**, *128*, 16876−16883.
(59) Talu, O.; Myers, A. L. *Colloids Surf., A* **2001**, *187*−*8*, 83−93.
(60) Talu, O.; Myers, A. L. *AIChE J.* **2001**, *47*, 1160−1168.
(61) Platt, G. K. *Space Vehicle Low Gravity Fluid Mechanics Problems and the Feasibility of their Experimental Investigation*, Nasa technical report, 1967.
(62) Sheinina, A. A.; Bereznyak, N. G.; Vorob'eva, V. P.; Khazhmuradov, M. A. *Low Temp. Phys.* **1993**, *19*, 356−364.
(63) Yakub, E. S. *Int. J. Thermophys.* **2001**, *22*, 505−516.
(64) Mccarty, R. *Hydrogen technology survey: thermophysical properties*, Nasa technical report, 1975.
(65) Peterson, V. K.; Liu, Y.; Brown, C. M.; Kepert, C. J. *J. Am. Chem. Soc.* **2006**, *128*, 15578−15579.
(66) Brown, C. M.; Liu, Y.; Yildirim, T.; Peterson, V. K.; Kepert, C. J. *Nanotechnology* **2009**, *20*, 204025.
(67) Grosch, J. S.; Paesani, F. *J. Am. Chem. Soc.* **2012**, *134*, 4207−4215.
(68) Cirera, J.; Sung, J. C.; Howland, P. B.; Paesani, F. *J. Chem. Phys.* **2012**, *137*, 054704.
(69) Paesani, F. *Mol. Simul.* **2012**, *38*, 631641.
(70) Rowsell, J. L. C.; Yaghi, O. M. *J. Am. Chem. Soc.* **2006**, *128*, 1304−1315.
(71) Rowsell, J. L. C.; Millward, A. R.; Park, K. S.; Yaghi, O. M. *J. Am. Chem. Soc.* **2004**, *126*, 5666−5667.
(72) Ma, S.; Sun, D.; Ambrogio, M.; Fillinger, J. A.; Parkin, S.; Zhou, H.-C. *J. Am. Chem. Soc.* **2007**, *129*, 1858−1859.
(73) Dinca, M.; Yu, A. F.; Long, J. R. *J. Am. Chem. Soc.* **2006**, *128*, 8904−8913.

(74) Sun, D.; Ma, S.; Ke, Y.; Collins, D. J.; Zhou, H.-C. *J. Am. Chem. Soc.* **2006**, *128*, 3896−3897.
(75) Wu, H.; Yao, K.; Zhu, Y.; Li, B.; Shi, Z.; Krishna, R.; Li, J. *J. Phys. Chem. C* **2012**, *116*, 16609−16618.
(76) McLaughlin, K.; Cioce, C. R.; Belof, J. L.; Space, B. *J. Chem. Phys.* **2012**, *136*, 194302.

## ■ NOTE ADDED AFTER ASAP PUBLICATION

This article was published ASAP on April 25, 2013 without the accompanying Supporting Information. The corrected version was published on April 26, 2013.